Identification and real-time imaging of a myc-expressing neutrophil population during inflammation and mycobacterial granuloma formation in zebrafish

Meijer, A.H.; Sar, A.M. van der; Cunha, C.; Lamers, G.E.M.; Laplante, M.A.; Kikuta, H.; ... ; Spaink, H.P.

Developmental and Comparative Immunology (2008) **32**, 36–49

Available at www.sciencedirect.com

ScienceDirect

journal homepage: www.elsevier.com/locate/devcompimm

Identification and real-time imaging of a *myc*-expressing neutrophil population involved in inflammation and mycobacterial granuloma formation in zebrafish

Annemarie H. Meijer[a,*,1], Astrid M. van der Sar[b,1], Cristiana Cunha[a], Gerda E.M. Lamers[a], Mary A. Laplante[c], Hiroshi Kikuta[c], Wilbert Bitter[b], Thomas S. Becker[c], Herman P. Spaink[a]

[a]*Institute of Biology, Leiden University, Wassenaarseweg 64, 2333 AL Leiden, The Netherlands*
[b]*Department of Medical Microbiology, VU Medical Centre, Van der Boechorststraat 7, 1081 BT Amsterdam, The Netherlands*
[c]*Sars International Centre for Marine Molecular Biology, University of Bergen, Thormøhlensgt. 55, N-5008 Bergen, Norway*

Received 26 February 2007; received in revised form 5 April 2007; accepted 6 April 2007
Available online 22 May 2007

KEYWORDS
Danio rerio;
Myeloid development;
Neutrophils;
Myc genes;
Inflammation;
Infectious disease;
Mycobacterium;
Transgenic model

Abstract
By enhancer trap screening we identified a transgenic zebrafish line showing leukocyte-specific YFP expression during late embryo and early larval development. Its enhancer detection insertion was mapped near a novel member of the *myc* proto-oncogene family, encoding transcription factors known to be important for regulating human myelopoiesis. Characterization of the zebrafish *myc* family showed that only this particular *myc* gene is strongly expressed in leukocytes. To identify the myc/YFP-expressing cell type, we re-examined specificity of described myeloid markers by multiplex fluorescent in situ hybridization, showing that *lcp1* can be considered as a general leukocyte marker, *csf1r* as a macrophage-specific marker, and *mpx* and *lyz* as neutrophil-specific markers. Subsequent colocalization analysis defined the YFP-positive cells as a subset of the neutrophil population. Using real-time confocal imaging we demonstrate that these cells migrate to sites of inflammation and are involved in innate immune responses towards infections, including *Mycobacterium marinum*-induced granuloma formation.

1. Introduction

Transparent zebrafish embryos are an attractive model for studying the development of myeloid cells and their

*Corresponding author. Tel.: +31 71 5274927; fax: +31 71 5274999.
E-mail address: a.h.meijer@biology.leidenuniv.nl (A.H. Meijer).
[1]These authors contributed equally to this work.

0145-305X/$ - see front matter © 2007 Elsevier Ltd. All rights reserved.
doi:10.1016/j.dci.2007.04.003

function in inflammation and infection [1–4]. Similar as in mammals, myelopoiesis in zebrafish is genetically controlled by expression of the PU.1 (Spi1) transcription factor [5]. PU.1-expressing myeloid precursors are first detected in zebrafish embryos at 12 h after fertilization and spread over the yolk sac during the first day of development [6]. Subsequently, PU.1 expression is down-regulated and myeloid precursors differentiate into macrophages and neutrophils (heterophils), recognizable by distinct morphological characteristics and specific marker gene expression [7–12]. Phagocytic activity of zebrafish macrophages has been observed as early as 1-day post-fertilization (dpf) [7]. Furthermore, neutrophilic inflammation in response to tissue injury was demonstrated in embryos from 2 dpf [11,12]. Since the adaptive immune system is not mature until several weeks after fertilization [8,13,14], the zebrafish embryo is particularly suitable for functional analysis of the innate immune system. For example, the use of a zebrafish embryo model for mycobacterial infection demonstrated that innate immunity determinants are sufficient for the typical response to this type of infection, since infected macrophages were observed to aggregate into characteristic granulomas [15].

To optimally exploit the possibilities of the zebrafish embryo model for real-time visualization studies there is a need for transgenic lines with fluorescent marker gene expression in different myeloid cell types. The zebrafish *pu.1/spi1* promoter was used to construct transgenic lines that express green fluorescent protein (GFP) in myeloid precursors at 1 dpf [16,17]. Furthermore, *fli1:EGFP* transgenic fish express GFP in the embryonic vascular system and can also be used to image early myeloid precursors [18,19]. Transgenic fish expressing GFP under control of the neutrophil-specific *myeloperoxidase* (*mpx*) promoter were also recently reported [20,21]. Further additions to the toolbox of distinct myeloid-specific transgenic marker lines will be extremely useful.

Enhancer detection, also named enhancer trapping, is a powerful method to identify tissue- or cell type-specific transgenic marker lines and has been successfully used in different animals and plants [22,23]. Enhancer detection vectors are designed to contain a basal (minimal) promoter upstream of a reporter gene. Upon insertion of the vector into the genome, reporter gene expression can be activated by nearby *cis*-regulatory elements. In many cases reporter gene expression faithfully mimics the expression pattern of an endogenous gene that is controlled by the same *cis*-regulatory elements that activate the enhancer detection cassette. Therefore, enhancer detection screening is a useful strategy for gene discovery as well as for the identification of novel marker lines. The first large-scale enhancer detection screen in a vertebrate organism was recently performed in zebrafish [24]. A murine retroviral vector (CLGY) containing a basal *gata2* promoter and a yellow fluorescent protein (YFP) reporter gene was used to generate a collection of transgenic zebrafish showing reporter expression in distinct patterns during embryonic development.

Here we screened the CLGY enhancer trap collection for lines expressing YFP in cells of the myeloid lineage. This screen resulted in the identification of line CLGY463, which expresses YFP in leukocytes, showing strongest intensity between 2 and 3 dpf. The insertion was mapped close to a novel member of the *myc* family of proto-oncogenes. This *myc* gene shows an expression pattern that closely resembles the YFP pattern, strongly suggesting that its *cis*-regulatory elements activate the nearby integrated enhancer detection cassette. We show that the YFP-positive leukocytes in CLGY463 belong to a newly identified neutrophil subpopulation and participate in the inflammatory response to wounding. Furthermore, we report on real-time analyses of the cellular response to non-pathogenic and pathogenic bacterial infections. In particular, analysis of *Mycobacterium marinum* infection revealed that YFP-positive neutrophils were associated with the typical formation of granulomas, where mycobacteria survive inside macrophages. Since the role of neutrophils in mycobacterial infection is not well understood, this finding adds to the versatility of the zebrafish embryo model for studying cellular-mediated determinants of tuberculosis.

2. Materials and methods

2.1. Identification of the enhancer trap line and mapping of the transgene

Generation of the CLGY enhancer trap collection and the linker-mediated PCR method for determination of a flanking genomic sequence of the activated viral insertion were previously described [24,25].

2.2. Phylogenetic analysis

Settings for Clustal W analysis (http://hypernig.nig.ac.jp) were as described [26]. Results were printed in the form of an unrooted rectangal cladogram using the program Treeview (http://taxonomy.zoology.gla.ac.uk/rod/treeview.html).

2.3. Manipulation of zebrafish embryos

Zebrafish (*Danio rerio*) were handled in compliance with the local animal welfare regulations and maintained according to standard protocols (http://ZFIN.org). Embryos were grown at 28 °C in egg water (60 μg/ml Instant Ocean see salts) containing 0.003% 1-phenyl-2-thiourea (Sigma) to prevent melanization. For the tail wounding assay, bacterial injections and microscopic imaging, embryos were kept under anesthesia in egg water containing 0.02% buffered 3-aminobenzoic acid ethyl ester (tricaine, Sigma). Bacterial injections were controlled using a Leica MZ Fluo 3 stereomicroscope with epifluorescence attachment, a Femtojet microinjector (Eppendorf) and a micromanipulator with pulled microcapillary pipettes.

2.4. In situ hybridization and immunodetection

cDNA clones of myeloid marker genes (*csf1r*, CD759443; *lcp1*, BC062381; *lyz*, BG883724; *mpx*, BC056287) and of *mych* (CA470797) were obtained from RZPD (http://www.rzpd.de/) and used to generate templates (1–2 kb) for riboprobe synthesis by PCR using gene specific primers

including binding sites for T3 or T7 RNA polymerases (*csf1r*, ATTAACCCTCACTAAAGGGACTGGACATGAGACCAGTCACATC, TAATACGACTCACTATAGGGTTGGGTTTAGACTGGGATCATAC; *lcp1*, ATTAACCCTCACTAAAGGGACGTCCATCTGCAGGTGATCATCA, TAATACGACTCACTATAGGGTGTGTAGCGGCATCTCAACATGT; *lyz*, ATTAACCCTCACTAAAGGGAGATAAAGCAGATATCAGCAGTGATAC, TAATACGACTCACTATAGGGCAATTTAGGAAGATGCTTTAATATTC; *mpx*, ATTAACCCTCACTAAAGGGAGTATCGAACTGCCAGCGGTGTCT, TAATACGACTCACTATAGGGACGGTCTCCTCTCTGTAGGCTCA; *mych*, ATTAACCCTCACTAAAGGGACGACCGCTTAAAACTGGAGGACT, TAATACGACTCACTATAGGGCCTGTCGCTCTCGGAGTTTGTCT). Templates for probes of other *myc* genes were amplified from genomic DNA (primers: *cmyca*: ATTAACCCTCACTAAAGGGATGTGGTGACTGTGGAAAAGCGACAG, TAATACGACTCACTATAGGGGAGAACACATAGCTAATACAGGTTC; *cmycb*: ATTAACCCTCACTAAAGGGAGATGAAGATGAAGAAGAGGAGGAAG, TAATACGACTCACTATAGGGCAACAGAATCTTGAATACATATGTG; *mycn*: ATTAACCCTCACTAAAGGGACTTACTCCGAACAGCAAGACGTTC, TAATACGACTCACTATAGGGAGGCAGACTTGAGTGTACGTTCTC; *mycl1a*: ATTAACCCTCACTAAAGGGAGATGACGATGAGGATGATGATGAG, TAATACGACTCACTATAGGGATCTCTGTGCAGTCGAGTAGATAC; *mycl1b*: ATTAACCCTCACTAAAGGGATGACGAAGAGATTGATGTGGTGAC, TAATACGACTCACTATAGGGGAGTCTCCTTAGTAGCTGCTGTTG). Digoxigenin- or fluoresceine-labeled riboprobes were generated using the labeling mixes from Roche and Ambion MEGAscript reagents for in vitro transcription.

Whole-mount in situ hybridization using alkaline phosphatase detection with BM Purple substrate (Roche) was carried out according to Thisse et al. [27].

Colocalization experiments by means of whole-mount fluorescent in situ hybridization were carried out using the multiplex FISH procedure described by Clay and Ramakrishnan [28]. Modifications to increase sensitivity were that probe concentrations were increased up to 1000 ng per 200 μl hybridization buffer and that concentrations of the primary antibodies for digoxigenin and fluoresceine were increased up to 1:1000. Furthermore, for tyramide signal amplification (TSA) detection, we replaced in some experiments the Alexa Fluor 555 and 488 tyramide reagents (Molecular Probes) with TSA Plus Cy3 and TSA Plus fluoresceine reagents (Perkin Elmer).

For immunodetection of YFP or *Salmonella* bacteria, embryos were fixed and permeabilized by methanol and proteinase K treatments in the same way as for in situ hybridization. Subsequently, embryos were incubated for 2 h in blocking buffer (10% goat serum, 1% DMSO, 0.1% Tween20, 0.8% Triton X-100) and incubated overnight in the first antibody, diluted in blocking buffer. First antibodies were a rabbit anti-GFP polyclonal antibody (TP401, Torrey Pines BioLabs) in 1:500 dilution and a rabbit anti-*Salmonella* αR60 polyclonal antibody (K196 G40, kindly provided by H. Brade) in 1:50 dilution. Embryos were then washed six times for 30 min in PBT (PBS+0.1% Tween 20), incubated for 2 h in blocking buffer, incubated overnight in 1:200 dilution of Alexa Fluor 488 goat anti-rabbit IgG (Molecular Probes) in blocking buffer, followed by six 30 min washes in PBT.

For colocalization of fluorescent in situ hybridization (FISH) signal with immunodetection of YFP or *Salmonella* bacteria, the FISH procedure described by Welten et al. [29] was applied, using Alexa-Fluor 555 tyramide or TSA Plus Cy3 as substrate for the horseradish peroxidase-conjugated sheep anti-digoxigenin antibody. Immunodetection of YFP or *Salmonella* was performed directly after the FISH procedure as described above.

2.5. Microscopy and image analysis

A Zeiss axioplan microscope with BIORAD MRC1024ES scanhead was used for confocal imaging of FISH and immunostaining experiments. Signals in the green and red channels were scanned sequentially using, respectively, the 488 nm laser line with 522 DF32 filter for detection of emitted light, and the 568 nm laser line with 605 DF32 filter for detection of emitted light. PLAN-NEOFLUAR objectives with the following specifications were used: 5 × NA 0.15 (Fig. 1A), 10 × NA 0.30 (Fig. 1B–D), 20 × NA 0.50 (Fig. 1J, inset in Fig. 1B, Fig. 4, Fig. 6F,G).

A Leica DMIRBE inverted microscope with a Leica SP1 confocal scanhead was used for confocal imaging of living embryos, which were placed in 8-well Lab-Tek II chambered coverglasses (Nunc). During real-time infection studies, CFP and YFP signals were completely separated by sequential scanning using respectively the 457 nm laser line with detection of emitted light between 466 and 500 nm, and the 514 nm laser line with detection between 530 and 590 nm. YFP and mCherry signals were completely separated by sequential scanning using, respectively, the 514 nm laser line with detection of emitted light between 527 and 572 nm, and the 568 nm laser line with detection between 588 and 800 nm. 10 × NA 0.40 (Fig. 5 and Supplemental movie 3) or 20 × NA0.70 (Fig. 1E–I, Fig. 6A–E,H–J, Supplemental movies 1,2,4–7) HC PLAN APO objectives were used.

Colors of confocal images were assigned using Image J (http://rsb.info.nih.gov/ij/) lookup tables. Image J or Adobe Photoshop were used to adjust brightness and contrast and to merge images for analysis of colocalization. No non-linear adjustments were perfomed. Z-stacks (maximum intensity) were made in Image J. Composite pictures of overlapping images were made using Adobe Photoshop (Fig. 1B–D). The resolution of the image shown in Fig. 6D was enhanced by deconvolution using the maximum likelihood estimate method in the Huygens software package (SVI, Hilversum, The Netherlands). Tracking analysis was performed manually using Image-Pro Plus version 6 (Media-Cybernetics). Supplemental movies were saved in audio video interleave format and compressed to Microsoft MPEG-4 Video Codec v2 format using Ulead GIF animator version 4.0.

Images of BM Purple-stained whole-mount in situ hybridizations were acquired with a Leica DC500 camera and MZ Fluo 3 stereomicroscope and composite images were made of different focal planes using Adobe Photoshop.

2.6. Bacterial strains

Infection experiments were performed using *Escherichia coli* DH5α containing the CFP-vector pMP4517 [30], *S. typhimurium* wild type strain SL1027 containing a modified pRSET-B-mCherry vector [31] with the sequence 5′- AAGCTTGAGGAGGAGATCC-3′ inserted between the BamHI site and the ATG of mCherry in order to provide a good Shine-Dalgarno sequence, and *M. marinum* strain Mma11 [32] containing the

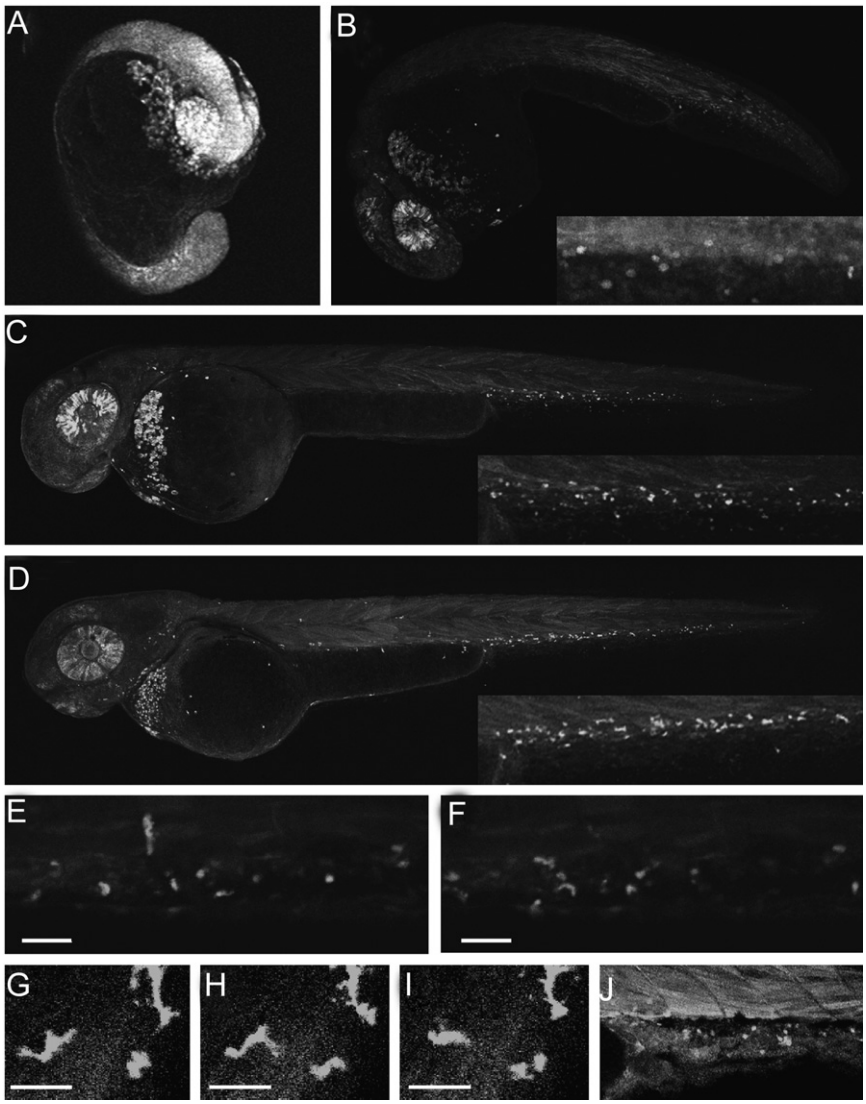

Fig. 1 Expression pattern of the CLGY463 YFP enhancer trap line. (A–D) Summed Z stacks of consecutive confocal images through CLGY463 embryos at the 16 somite stage (A), 24 hpf (B), 2 dpf (C) and 3 dpf (D), stained by immunohistochemistry for YFP using an Alexa488-conjugated 2nd antibody. The inset in (B) shows the ventral tail region of a 30 hpf embryo. The insets in (C) and (D) show enlargements of the ventral tail regions above. (E–F) Two frames with 62 min time interval taken from a 9 h time lapse movie of the venous plexus in the ventral tail region of a 3 dpf CLGY463 embryo (Supplemental movie 1). (G–I) Three frames with 1 min time intervals taken from a 4 min time lapse movie of a 3 dpf CLGY463 embryo, zoomed in at leukocytes in the musculature above the venous plexus (Supplemental movie 2). J. Summed Z stacks of consecutive confocal images through the venous plexus in the ventral tail region of a CLGY383 embryo at 3 dpf, stained by immunohistochemistry for YFP as in (A–D). Line CLGY383 has an enhancer trap insertion close to that of line CLGY463 as shown in Fig. 2A. A whole-mount image of CLGY383 at 24 hpf is shown by Ellingsen et al. [24]. All embryos are oriented anterior to the left and dorsal to the top. Bars in E,F: 50 μm; bars in G–I: 10 μm.

pSMT3-mCherry vector. pSMT3-mCherry was constructed by cloning mCherry digested from the modified pRSET-B-mCherry with *Bam*HI and *Eco*RV into the *Bam*HI and *Nae*I sites of pSMT3-eGFP [33].

3. Results

3.1. Identification of YFP enhancer trap lines expressing in leukocytes

The CLGY enhancer trap collection [24] was screened to obtain novel transgenic zebrafish lines with YFP reporter expression in myeloid cell types. Screening of embryos at 1–3 dpf from 58 independent transgenic lines resulted in the identification of 3 candidate lines, named CLGY463, CLGY746 and CLGY869. Line CLGY 746 showed YFP-expression in cells migrating on the yolk sac between 1 and 2 dpf, resembling the pattern of available PU.1-GFP lines [16,17]. In CLGY 869, YFP expression was also detected in erythrocytes. We selected line CLGY463 for further characterization because its expression pattern appeared different from any previously described marker lines [16,17,20,21]. From somitogenesis stages until 1 dpf, CLGY463 shows ubiquitous YFP expression, with strongest signals in the eye, midbrain and hatching gland (Fig. 1A,B). At 1 dpf, some YFP-positive

putative myeloid precursors can be observed on the yolk sac, in the blood island and ventral tail region (Fig. 1B), but the background YFP expression in other tissues is also high. However, embryos of 2 and 3 dpf show a more restricted YFP expression pattern (Fig. 1C, D). Corresponding to described distribution patterns of myeloid cell types [7,9,11,12,34], many strongly YFP-positive cells in 2–3 dpf embryos are accumulated in the tissue around the caudal vein plexus, some are scattered over the yolk sac, and some are observed near the otic vesicle and in the somites. Other domains of strong YFP expression have become restricted to the retinal growth zones, the forebrain and midbrain and the hatching gland. Time lapse imaging of the venous plexus region showed several YFP-positive cells actively migrating through the tissue (Fig. 1E, F and Supplemental movie 1), indicating that these cells are leukocytes and not thrombocytes, which also accumulate in the venous plexus [35]. Occasional movement of YFP-positive cells in the bloodstream was also observed. Higher-resolution imaging showed a highly branched and dynamic morphology (Fig. 1G–I and Supplemental movie 2). The YFP expression level in leukocytes of CLGY463 peaks around 2.5–3 dpf, with up to 60 cells being detectable by live confocal imaging and 100–150 by YFP immunostaining (Fig. 1D). After 3 dpf, the total number of fluorescent cells and their average intensity decreased gradually, but up to 20 cells remained detectable until at least 6 dpf, usually in small clusters of ca. 5 cells. In conclusion, the YFP-insertion in CLGY463 appears to detect an enhancer activity that regulates expression in leukocytes during a specific time window.

3.2. Genomic mapping of the CLGY463 insertion close to a member of the myc gene family

The flanking sequence of the insertion in CLGY463 was determined and used to search the Zv6 zebrafish genome assembly in the Ensembl database (http://www.ensembl.org) using BLASTN. A single unique hit was found, mapping the insertion at 1.8 kb upstream of an ab initio prediction (FGENESH00000055905), showing homology to members of the *myc* family of proto-oncogenes (Fig. 2A). The encoded protein contains both the conserved amino-terminal region (pfam01056) and the helix–loop–helix domain (cd00083, smart00353) characteristic for Myc family members. Another viral insertion (CLGY383) was mapped 2.6 kb downstream of the predicted *myc* gene (Fig. 2A) [24]. Similar to CLGY463, CLGY383 shows strongest YFP expression in eye, brain and hatching gland at 1 dpf [24]. At 2–3 dpf, CLGY383 also shows YFP expression in leukocytes (Fig. 1J), but higher background expression in other tissues makes this line less useful for leukocyte analysis than CLGY463. No other genes or predictions are present within more than 100 kb upstream and 38 kb downstream of the CLGY463/CLGY383 insertions and whole mount in situ hybridization showed that the expression pattern of the *myc* gene resembles the YFP pattern of the CLGY463/CLGY383 lines (Fig. 3A). Like the YFP pattern, *myc* gene expression is strong in the eye and brain, and at 2–3 dpf clearly marks cells accumulated around the caudal vein plexus and some cells on the yolk sac or within tissues. Different from the YFP pattern, strong expression in the hatching gland was not observed. The *myc* gene expression pattern was undistinguishable between wild type and CLGY463 transgenics (Fig. 3A), indicating that the upstream viral insertion does not affect the normal *myc* expression pattern.

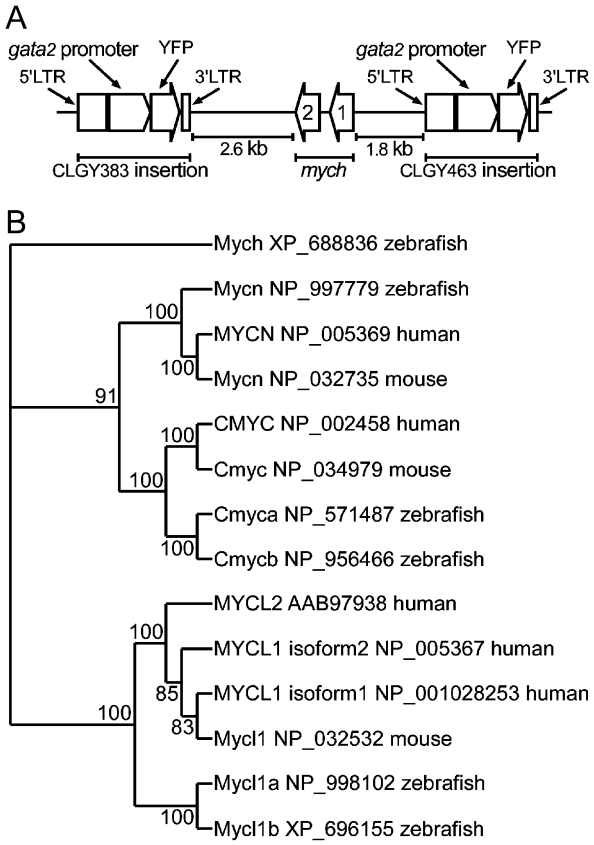

Fig. 2 Association of the CLGY463 insertion with a member of the *myc* gene family. (A) Genomic organization of the *mych* gene on chromosome 6 and orientation of the upstream viral insertion in transgenic line CLGY463, consisting of 5′ and 3′ LTRs (long terminal repeats), a basal *gata2* promoter and a YFP reporter gene. In addition, the orientation of the viral insertion in transgenic line CLGY383 is shown. (B) Unrooted phylogenetic tree based on ClustalW alignment of the full-length human, mouse and zebrafish Myc proteins. The numbers indicate the occurrence of nodes during bootstrap analysis, given as percentages of 10,000 reiterations. Human MYCL2 is derived from a pseudogene. Genbank accession numbers of reference sequences used for the alignment are indicated in the figure.

3.3. Characterization of the zebrafish myc family

The *myc* homolog near the CLGY463/383 insertions is annotated in the ZFIN database (http://ZFIN.org) as a gene (ZDB-GENE-030219-51, id:ibd5144) characterized solely by a collection of ESTs (unigene cluster Dr.56441). Other *myc* genes annotated in ZFIN include putative orthologs of the three members of the human *MYC* family, *CMYC*, *MYCN* and *MYCL1* (Table 1). To characterize the entire zebrafish Myc family we used the known zebrafish and human Myc protein sequences to search the zebrafish assembly using TBLASTX and determined that the zebrafish Myc family consists of 6

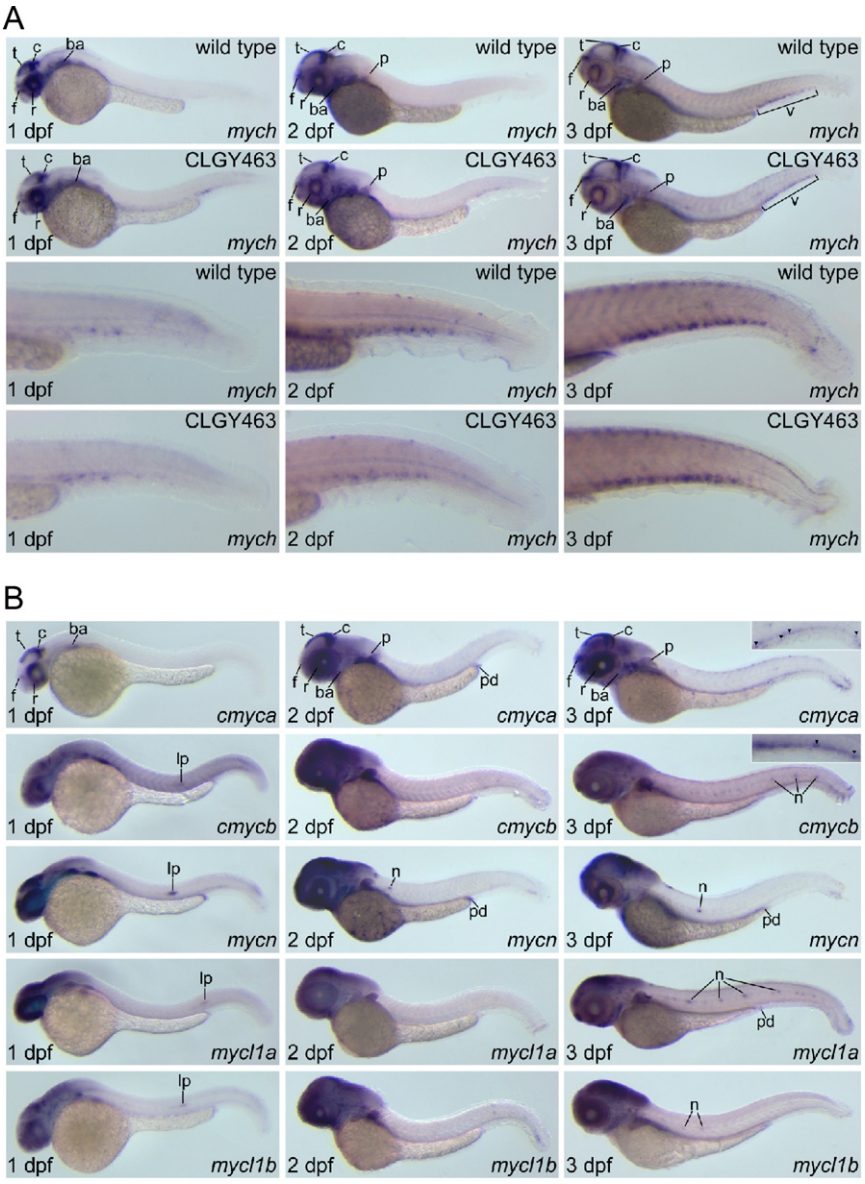

Fig. 3 Expression patterns of the members of the *myc* gene family. (A) Whole mount in situ hybridizations of wild type embryos (1st row) and CLGY463 transgenic embryos (2nd row) at 1, 2 and 3 dpf with an antisense probe of the *mych* gene that maps close to the CLGY463 insertion. Tail details of wild type (3rd row) and CLGY463 transgenics (4th row) show expression in cells in the region of the venous plexus associated with the caudal vein. This expression is first observed around 36 hpf and is much weaker at 1–2 dpf than expression in eye and brain. Therefore, the tail details shown are of different embryos stained longer than the embryos in the rows above. At 3 dpf, staining intensity of cells in the venous plexus was similar to staining in the eye and brain regions. (B) Whole mount in situ hybridizations of wild type embryos at 1, 2 and 3 dpf with antisense probes of *cmyca* (1st row), *cmycb* (2nd row), *mycn* (3rd row), *mycl1a* (4th row) and *mycl1b* (5th row). The *Cmyca* and *cmycb* genes show diffuse expression in the venous plexus region at 3 dpf. A magnification of this region is shown in the insets and possible leukocytes showing slightly higher expression than the surrounding tissue are indicated with arrowheads (inset of *cmycb* is from a different embryo stained longer). Note the difference with the more specific expression of *mych* in cells in the venous plexus region (Fig. 3A). All embryos are oriented anterior to the left and dorsal to the top. ba, branchial arches; c, cerebellum; f, forebrain ventricular zone; lp, lateral line primordium; n, neuromast; p, pectoral fin bud; pd, pronephric duct; r, retina; t, tectum; v, venous plexus region.

members (Table 1). A phylogeny reconstruction places the Myc homolog identified by the CLGY463 insertion on a separate branch, while the other zebrafish Myc proteins group with the human CMYC, NMYC or MYCL1 proteins (Fig. 2B). Supported by the phylogenetic tree and synteny between chromosomal segments in zebrafish, we conclude that zebrafish contains two duplicated *cmyc* genes (renamed *cmyca* and *cmycb*), a single *mycn* copy, two duplicated *mycl1* genes (renamed *mycl1a* and *mycl1b*) and a distant *myc* gene, named *mych* (for *myc homologous*), which is the gene tagged by the CLGY463/CLGY383 insertions.

Table 1 Overview of the zebrafish *myc* gene family

Gene symbol[a]	Previous symbol	ZFIN ID	Ensembl ID	Genomic location	Reference sequence[b]	Peptide ref seq	Unigene cluster
cmyca	*cmyc*	ZDB-GENE-990415-162	ENSDARG 00000045695	Chr.24 CT573344.3	NM_131412	NP_571487	Dr.1
cmycb	*zgc:55680*	ZDB-GENE-040426-780	ENSDARG 00000007241	Chr.2 CR391940.14	NM_200172.1	NP_956466	Dr.78260
mycn	*mycn*	ZDB-GENE-020711-1	ENSDARG 00000006837	Chr.20 BX005358.16	NM_212614.1	NP_997779.1	Dr.75499
mycl1a	*mycl1/ zgc:85967*	ZDB-GENE-020711-2/ZDB-GENE-040426-2439	ENSDARG 0000006003	Chr.13 BX510990.32	NM_212937.1	NP_998102.1	Dr.79747
mycl1b	–	ZDB-GENE-030131-5561	(ENSDARG 00000034956)[c]	Chr.19 BX547927.10	NM_001045142	NP_001038607	Dr.74192
mych	*id:ibd5144*	ZDB-GENE-030219-51	–	Chr.6 BX649289.11	XM_683744	XP_688836	Dr.56441

[a]The assigned gene symbols have been approved by the ZFIN nomenclature committee.
[b]For genes of which a reference sequence is unavailable the accession number of the predicted sequence is given instead.
[c]The Ensembl ID of *mycl1b* is between brackets because it represents an incorrect prediction of 4 instead of 2 exons.

In situ hybridizations of the other *myc* genes were performed to determine if these show similar leukocyte-specific expression as the *mych* gene (Fig. 3B). Only *cmyca* and *cmycb* show staining in some cells in the venous plexus region, but this is not very specific since these genes also show diffuse expression in the surrounding tissue. The *cmyca* expression pattern, previously described by Thisse et al. [36], is the most similar to that of *mych*. All *myc* genes are expressed in retina, tectum, cerebellum, forebrain, branchial arches and pectoral fin buds. However, *cmyca*, *mycn* and *mych* show a more spatially restricted expression pattern in the brain than *cmycb*, *mycl1a* and *mycl1b*. A detailed description of the brain-specific expression pattern of *mycn* was previously reported by Loeb-Hennard et al. [37]. Additionally, *mycn* shows strong expression in the lateral line primordium (1 dpf) and subsequently in specific lateral line neuromasts (2 and 3 dpf). Weaker expression in the lateral line primordium is detected with *cmycb*, *mycl1a* and *mycl1b* probes. Furthermore, *cmycb*, *mycl1a* and *mycl1b* also show expression in lateral line neuromasts. Expression in the pronephric duct is detected with *cmyca*, *mycn* and *mycl1a* probes. In conclusion, in situ hybridizations revealed that none of the other *myc* genes is as strongly expressed in leukocytes as the *mych* gene.

3.4. Characterization of the YFP-expressing myeloid cell type

To establish the identity of the YFP-expressing leukocyte population in CLGY463 we studied colocalization of YFP with myeloid cell markers. The literature describes *lcp1* (*L-plastin*), *lyz* (*lysozyme C*) and *csf1r* (colony stimulating factor 1 receptor, *fms*), as markers for macrophages, and *mpx* (myeloperoxidase, *mpo*) as a marker for neutrophils [7,9–11,38]. However, occasional coexpression between *lcp1* and *mpx* was also reported [9]. This prompted us to re-examine the specificity of these markers by means of two-color fluorescent in situ hybridization (multiplex FISH) [28] in 2-day-old embryos. Multiplex FISH analysis of *lcp1* and *mpx* expression revealed two populations of leukocytes, one coexpressing *lcp1* and *mpx* (ca. 40%) and the other expressing *lcp1* alone (ca. 60%) (Fig. 4A). Therefore, *lcp1* appears to be expressed in all leukocytes, while *mpx* marks a specific population, previously shown to display neutrophil characteristics [9,11]. *Lcp1* expression also overlapped partially with *csf1r* expression, which was previously shown to be expressed in macrophages and neural crest [10,39] (Fig. 4B). Expression of *csf1r* and *mpx* was found to be completely non-overlapping (Fig. 4C). Expression of *lyz* colocalized completely with *mpx*, and, like *mpx*, *lyz* showed no overlap with *csf1r* (Fig. 4D,E). Based on these observations we conclude that, at the examined stage of 2 dpf, *lcp1* can be used as a general leukocyte marker, *csf1r* as a marker for macrophages and neural crest, and either *lyz* or *mpx* as markers for neutrophils. Subsequently, analysis of CLGY463 embryos at 2 dpf showed that YFP immunostaining colocalized with a subset (ca. 50%) of cells expressing *mpx* (Fig. 4F), indicating that the YFP-expressing cells possess neutrophil identity and probably represent a major subpopulation of neutrophils.

3.5. Inflammatory response to wounding

The *mpx*-expressing neutrophil population of zebrafish embryos was previously shown to accumulate at sites of trauma, using a caudal fin-clipping assay [11]. Based on the overlap between *mpx* and YFP expression in CLGY463, we used the same assay to test if the fluorescent leukocytes participate in the inflammatory response. Time-lapse imaging showed rapid migration of fluorescent leukocytes

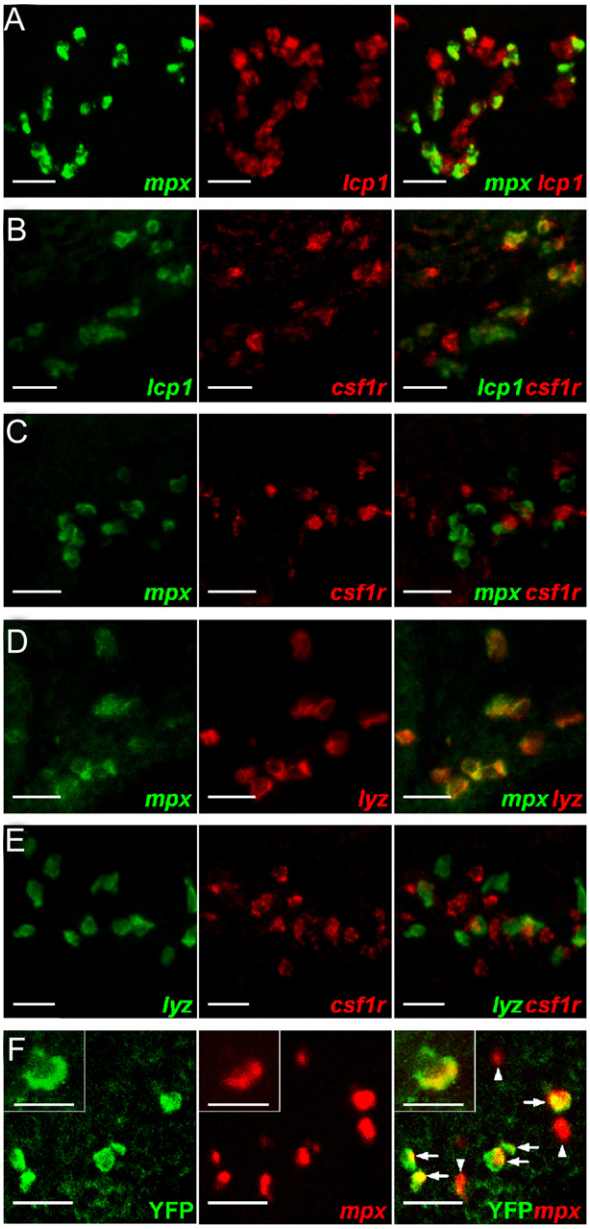

Fig. 4 Colocalization experiments with myeloid-specific marker genes. (A–E) Multiplex FISH with antisense probes of myeloid marker genes as indicated in the figures. Genes indicated in red are detected with digoxigenin-labeled probes and Alexa Fluor 555 tyramide (A) or TSA Plus Cy3 (B–E) labeling. Genes indicated in green are detected with fluorescein-labeled probes and Alexa Fluor 488 tyramide (A) or TSA Plus fluoresceine labeling (B–E). (F) Colocalization in line CLGY463 of FISH signal for *mpx*, detected with a digoxigenin-labeled probe and Alexa Fluor 555 tyramide labeling, and immunostaining for YFP, detected with an Alexa Fluor 488-conjugated antibody. Arrows indicate colocalizing cells, arrowheads indicate cells in which only *mpx* expression is detected. The inset shows a magnification of another example of a colocalizing cell. All images show summed Z stacks of consecutive confocal images through the venous plexus region in the ventral part of the tail of 2 dpf embryos. Each panel shows from left to right the signal recorded in the green channel, the signal recorded in the red channel, and the merged image. Bars in (A–F) 20 μm, bar in inset of (F) 10 μm.

to wounding sites. One example of a 13 h time lapse movie is shown in Fig. 5 and Supplemental movie 3. At the start of this movie (20 min after wounding) only 1 cell was observed in the caudal fin tissue posterior of the notochord, while approximately 35 cells had migrated into this area after 13 h, most of which were at the edge of the wounding site (Fig. 5B–E). The majority of these leukocytes had migrated from the ventral side of the tail into the fin area, and only 4 cells had migrated along the dorsal side of the tail. Migrating cells changed shape rapidly and formed long protrusions (Fig. 5F–J). Cell tracking analysis showed that the first 3 migrating cells moved directly to the closest edge of the wound (Fig. 5K), while the next 3 cells migrated further to the distant edge (Fig. 5L). Several cells moved in small groups along similar tracks or followed part of the same tracks as other cells before them (Fig. 5M). Sometimes cells stopped and turned before continuing on a track to the wounding site (Fig. 5N). Some cells were observed to move through the tail veins or intersegmental vessels (Fig. 5O). An average speed of 4 μm/min was calculated from tracks of nine different cells migrating through the tissue along the ventral side of the tail during the first 200 min of the movie. Together, these experiments show that the YFP-expressing neutrophil subpopulation in CLGY463 indeed participates in the inflammatory response like previously demonstrated for *mpx*-expressing neutrophils [11].

3.6. Response to bacterial infections

To characterize the response of CLGY463 to infections we tested three bacterial models, including *E. coli*, which is non-pathogenic for zebrafish embryos [40], *Salmonella typhimurium*, a pathogen spreading through the blood vessels and lethal within 2 days [40], and *M. marinum*, which causes a characteristic infection with granuloma formation [15]. Bacteria were labeled with CFP or mCherry, which are both colors that can be separated completely from the YFP signal in leukocytes by confocal microscopy.

To study the short-term response to infections, bacteria were injected into the muscle tissue of embryos at 2–3 dpf, in the area above the caudal vein plexus where many YFP-positive leukocytes are accumulated. An example of the response to *E. coli* is shown in Fig. 6A–C and Supplemental movie 4. Shortly after injection, several YFP-positive cells were observed to arrive at the infection site (Fig. 6A,B). Furthermore, *E. coli* bacteria that were initially dispersed over the tissue (Fig. 6A) progressively became clustered over a period of several hours (Fig. 6B,C). These clusters moved through the tissue in a similar manner as the YFP-positive cells (Supplemental movie 4), indicating that the clustered bacteria were ingested by YFP-negative leukocytes. Confocal Z-series showed that some of the YFP-positive cells at infection sites also contained *E. coli* bacteria (Fig. 6D), indicating their capability of phagocytosis. Migration of YFP-positive cells to infected areas was also evident after injection of *S. typhimurium* or *M. marinum* bacteria. Time-lapse imaging and confocal Z-series showed evidence of YFP-positive cells carrying ingested bacteria in addition to the presence of YFP-positive cells without bacteria and bacteria clustered inside YFP-negative cells (Fig. 6E, Supplemental movies 5–7).

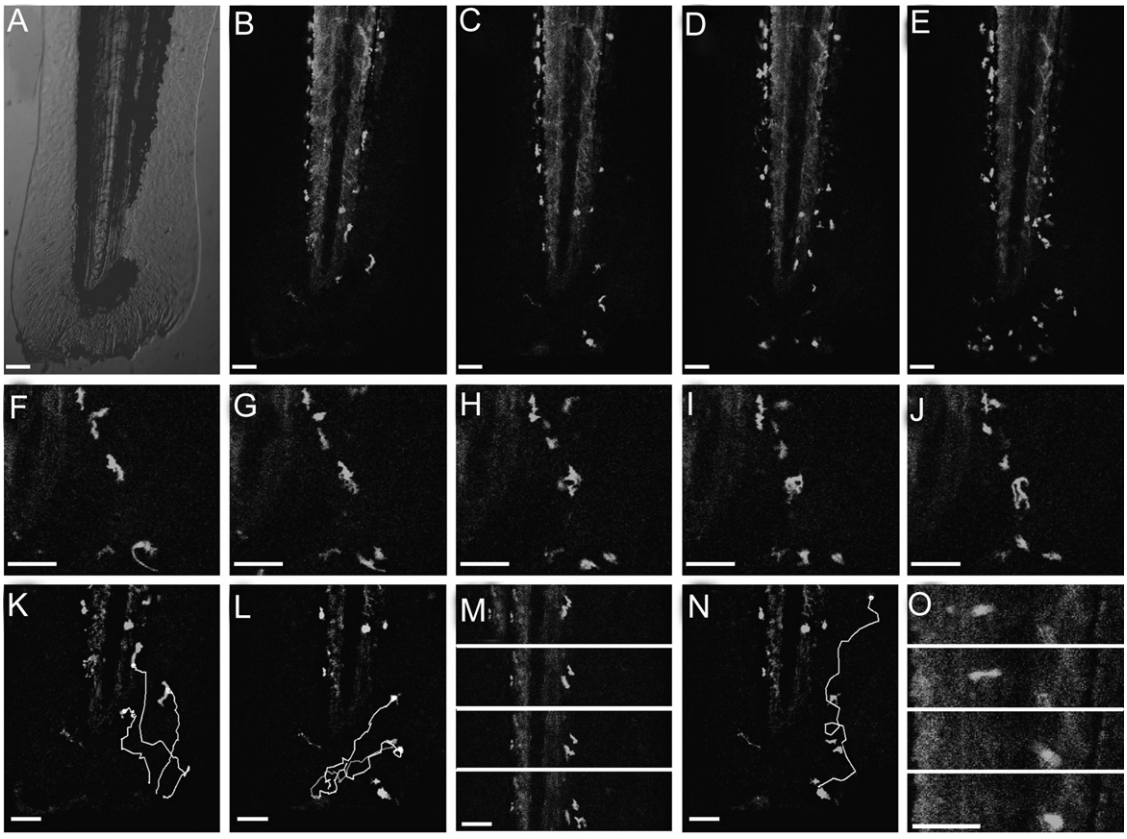

Fig. 5 Inflammatory response to wounding. (A) Bright field image showing the wounded area at the caudal fin of a 3 dpf CLGY463 embryo. (B–E). Four frames from a 13 h time lapse movie (Supplemental movie 3) of the inflammatory response to the wound shown in (A). The images show the progress of cell migration at 0 (B), 100 (C), 200 (D) and 400 min (E) from the start of time-lapse imaging (20 min after wounding). (F–J) Five frames with 2 min time intervals showing the dynamics of cell shapes at approximately 6 h after wounding. (K–L) Cell tracks during the first 100 min from the start of time lapse imaging, showing the first (K) and second (L) group of cells migrating to opposite edges of the wound. (M) Four frames with 4 min time intervals showing a group of cells migrating along a similar route. First frame at the top. (N) Example of a long track interrupted by a stop and turn. This track was covered in 64 min. (O) Four frames with 2 min time intervals showing movement of a fluorescent leukocyte through an intersegmental vessel. First frame at the top. Orientations are anterior to the top and dorsal to the left. Bars: 50 μm.

Therefore, more than one leukocyte cell type appeared to be active in phagocytosis. To obtain independent evidence for phagocytosis by different leukocyte cell types in embryos at 2–3 dpf, we studied colocalization of macrophage and neutrophil marker genes with ingested *S. typhimurium* bacteria. In agreement with the life imaging data, *S. typhimurium* bacteria were found to be present in different cell types, expressing the macrophage marker *csf1r* (Fig. 6F) and the neutrophil marker *mpx* (Fig. 6G).

Next we studied the long-term response to *M. marinum* infection. Bacteria were injected into the axial vein near the blood island at 1 dpf. At 5 days post-infection (dpi) characteristic aggregation of leukocytes into granuloma-like structures was observed (Fig. 6H–J). Davis et al. [15] previously showed that the structural organization of such leukocyte aggregates resembles that of adult granulomas and that granuloma-specific *Mycobacterium* genes are activated after their formation. The granulomas observed in CLGY463 consisted of multiple cell types, including cells that were full of bacteria but expressed no or low levels of YFP, cells that strongly expressed YFP but contained no bacteria, and cells showing clear colocalization of YFP and bacteria. Whole-mount in situ hybridization of *M. marinum*-infected wild type embryos confirmed the presence of different leukocyte cell types in granulomas. In wild type embryos, macrophages marked by *csf1r* expression and neutrophils marked by *mpx* expression were scattered over the ventral region of the tail (Fig. 6K,M). In contrast, cells expressing these markers were aggregated in *M. marinum*-infected embryos (Fig. 6L,N, Supplemental Fig. 1). Furthermore, *csfr1* and *mpx* staining developed faster in infected embryos, suggesting induced expression levels. In conclusion, life imaging using CLGY463 as well as marker analysis of wild type embryos indicated that cells expressing macrophage and neutrophil markers are associated with the granulomas formed in zebrafish embryos upon *M. marinum* infection.

4. Discussion

We have identified a transgenic zebrafish line (CLGY463) that permits real-time visualization of the response of a subpopulation of embryonic neutrophils to inflammation and

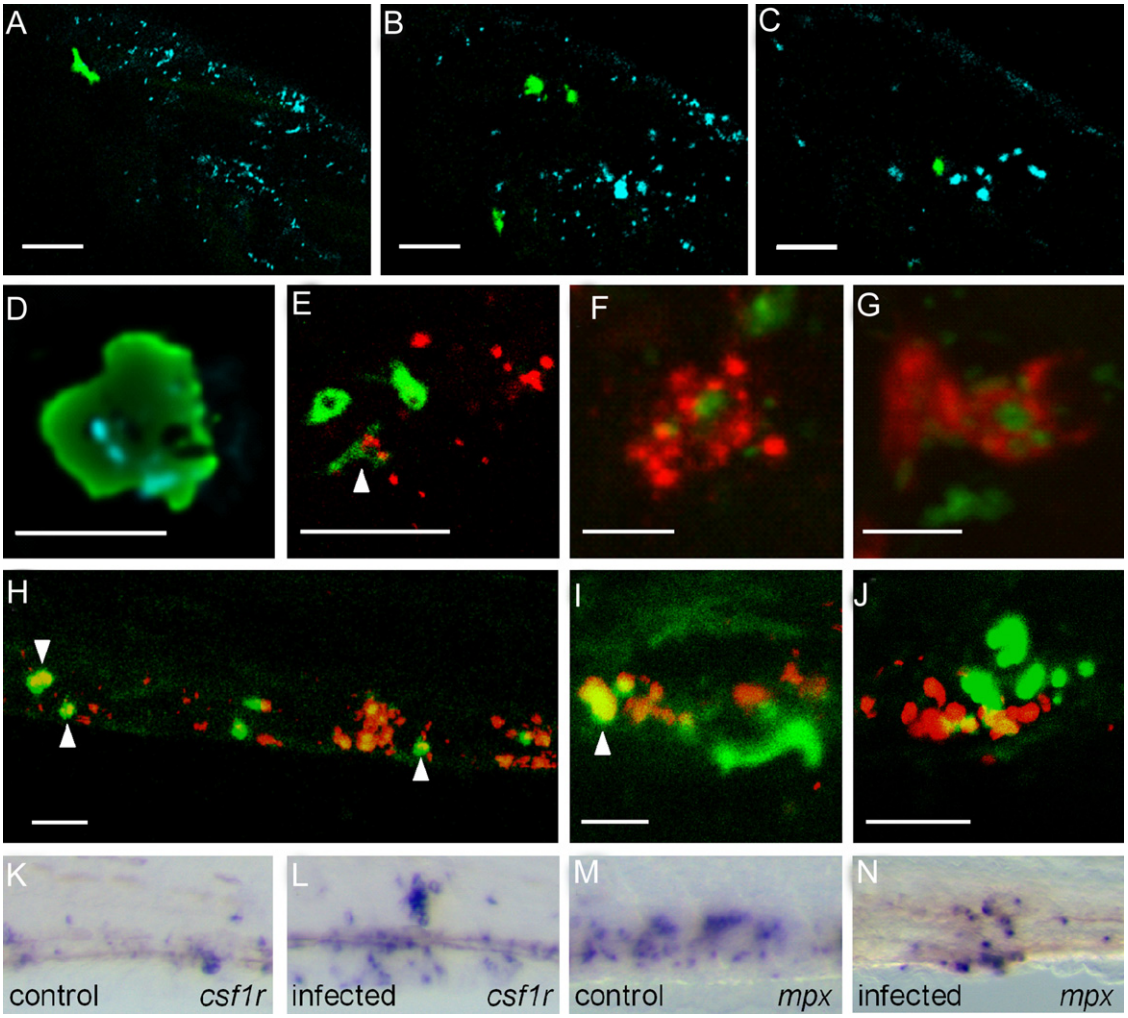

Fig. 6 Responses to *E. coli*, *S. typhimurium* and *M. marinum* infections. (A–C) Response of YFP-expressing leukocytes (green) to CFP-labeled *E. coli* bacteria (cyan) injected into the musculature above the caudal vein plexus of a 3 dpf CLGY463 embryo. Confocal images were taken at 20 min (A), 1.5 h (B) and 4 h (C) post-injection. A time lapse movie from 1 to 5 h post-injection is given as Supplemental movie 4. (D) CFP-labeled *E. coli* ingested by a YFP-expressing leukocyte in a 3 dpf CLGY463 embryo. The image is taken at 135 min post-injection and shows a single slice from a deconvolved confocal Z-series of 16 slices with 1 μm spacing. Imaging conditions were as in (A–C) except that the electronic zoom factor was increased. (E) Response of YFP-expressing leukocytes (green) to mCherry-labeled *S. typhimurium* bacteria (red) injected into the musculature above the caudal vein plexus of a 3 dpf CLGY463 embryo. The arrowhead indicates a YFP-expressing leukocyte that carries ingested bacteria as can be observed in Supplemental movie 5. (F–G) Colocalization of FISH signal for *csf1r* (F) or *mpx* (G) with immunostaining signal for *S. typhimurium*. FISH signals (red) were detected with digoxigenin-labeled probes and TSA-plus-Cy3 labeling, immunostaining of bacteria (green) was detected with an Alexa488-conjugated antibody. (H–J) Overview (H) and details (I,J) of the ventral tail regions of 6 dpf CLGY463 embryos at 5 days post-injection of mCherry-labeled *M. marinum* bacteria (red) into the bloodstream. Arrowheads indicate examples of leukocytes with strong YFP expression and containing ingested bacteria. (K–N) Parts of the ventral tail regions of 6 dpf control embryos and *M. marinum*-infected embryos stained by whole-mount in situ hybridization with antisense *csf1r* and *mpx* probes as indicated. Control embryos with *mpx* probe were stained 6 times longer than infected embryos. The infected embryo in N was sectioned to show that the region in the tail with *mpx*-positive cells contains a cell aggregate (Supplemental Fig. 1). The infection procedure was as in (H–J). All embryos are oriented anterior to the left and dorsal to the top. Bars in (A–C,E,H,J) 50 μm; (I) 20 μm; (F–G) 10 μm, (D) 5 μm.

infections. This neutrophil population was revealed by an enhancer detection insertion near a novel *myc* transcription factor gene. Neutrophil-specific YFP expression in CLGY463 peaks during 2 and 3 days of embryo development and is detectable until at least 6 days. This time window allows the analysis of responses to acute bacterial infections as well as to chronic infections, such as those observed in the *M. marinum* model for tuberculosis [15]. The transgenic line will also be useful for genetic or chemical screens to identify modulators of the immune response.

In all vertebrates, the process of blood cell formation occurs in two successive waves, called primitive and definitive hematopoiesis, and during development the hematopoietic locations shift several times before establishment of the adult hematopoietic organs [41]. In zebrafish embryos, primitive hematopoiesis takes place within the

first day of development [7,42]. During the second day, definitive hematopoiesis begins ventral to the trunk dorsal aorta, in a tissue equivalent with the hematopoietic aorta–gonad–mesonephros (AGM) area of mammals [13]. In CLGY463, strong YFP expression in myeloid cells is not detected until 2 dpf and declines after 3 dpf. Therefore, CLGY463 demonstrates the activity of an enhancer element that drives expression in a specific subpopulation of myeloid cells. The majority of these cells are located in the tissue around the caudal vein plexus. Herbomel and coworkers [34] recently identified this tissue as a transient site of definitive hematopoiesis that supports the accumulation, expansion and differentiation of AGM-derived blood precursors, prior to their further migration to the final hematopoietic organs. Thus, strongest enhancer activity of CLGY463 occurs in a population of cells developing in this newly described intermediate hematopoietic site, which was named the caudal hematopoietic tissue (CHT) [34].

Colocalization studies of YFP immunostaining with myeloid markers showed overlap of YFP with part of the population of cells that express the *mpx* gene. This gene has been reported as a neutrophil-specific marker [11]. We used a multiplex FISH procedure [28] to re-examine the specificity of several myeloid markers described in the literature. It is known that *lcp1* (*L-plastin*) is expressed in macrophages [7] and this gene has subsequently been used as macrophage-specific marker [21,38]. However, partial overlap with *mpx*-expressing cells has also been reported [9]. Our multiplex FISH analysis of *lcp1* and *mpx* in embryos at 2 dpf showed two populations of cells, one expressing *lcp1* alone and the other coexpressing *lcp1* and *mpx*. These data indicate that *lcp1* can be expressed in all leukocytes, and are consistent with the previous notion of *mpx* as a neutrophil-specific marker [11,12]. The specificity of *mpx* is confirmed by multiplex FISH data reported here and in a previous study [28], both showing a lack of overlap with *csf1r* (*fms*), which is expressed in macrophages and neural crest [10]. Furthermore, myeloperoxidase is a distinctive component of neutrophil granules in mammals [43]. Granules of mammalian neutrophils also contain abundant levels of lysozyme C (lyz) [43]. In agreement, our multiplex FISH analysis showed colocalization of *mpx* and *lyz* expression, while *lyz* and *csf1r* expression were non-overlapping. This contrasts with an earlier report of *lyz* as a macrophage-specific marker in zebrafish embryos [38]. Discrepancies in the literature concerning marker specificity indicate that cautiousness is needed using the described myeloid marker genes. In all cases, results can be dependent on the sensitivity of the detection method and the specific developmental stage examined. For example, we found *lcp1* expression in all leukocytes at 2 dpf, but a reduced expression in neutrophils at later stages might well explain that others did not find overlap between *lcp1* and *mpx* markers [21]. Since the specificity of *mpx* for zebrafish embryonic neutrophils remains undisputed, we conclude that the strong YFP-positive leukocytes in CLGY463 belong to the neutrophil lineage. However, we cannot exclude that weak YFP expression in cells of the macrophage lineage has remained undetected in our analyses. Furthermore, since YFP was not detectable in all *mpx*-expressing cells, there is an obvious need for additional markers that can distinguish different myeloid subsets or developmental stages.

The enhancer detection strategy used to identify CLGY463 led to the discovery of a novel member of the *myc* family of proto-oncogenic transcription factor genes [44], which we named *mych*. For several reasons it is likely that *mych*-associated *cis*-regulatory elements activate the enhancer detection cassette integrated 1.8 kb upstream. First, the majority of CLGY enhancer detection events were shown to occur over a distance of 15 kb or less [24] and no other genes are present near the CLGY463 insertion. Second, another nearby insertion (CLGY383) shows a similar pattern of reporter gene activation. Third, the *mych* and YFP reporter expression patterns are very similar. Genomic mapping of CLGY inserts previously indicated a bias towards detection of transcription factor genes involved in early development [24]. In this respect it is interesting to note that two insertions near other members of the *myc* family have been identified in the CLGY collection, of which the YFP patterns also mimic the endogenous gene expression (T. S. Becker, unpublished results). Previous reports [36,37] and data reported here showed that all six members of the zebrafish *myc* family are expressed in retinal growth zones and regions of the brain. Furthermore, some members are expressed in specific proliferating tissues, such as the lateral line primordium. Strong expression in leukocytes appears to be specific for *mych*, which is more distantly related to the human *MYC* genes (*CMYC*, *MYCN* and *MYCL1*) than any of the other five zebrafish *myc* genes. The expression of *mych* is not restricted to larval haematopoiesis, since we could also detect *mych* expression in cells of the adult kidney marrow (unpublished results). Human *MYC* genes play central roles in regulating cell proliferation [45,46]. Their repression is required for terminal differentiation of many cell types, including hematopoietic cells [45]. Repression of *CMYC* in human neutrophils was shown to be controlled by the CCAAT/enhancer binding protein α (C/EBPα) [47]. Since myeloid-specific expression of C/EBP genes is conserved in zebrafish embryos [48,49], it is possible that a similar pathway controls neutrophil differentiation in zebrafish. Future gain- and loss-of-function studies should clarify the role of *mych* in zebrafish neutrophil development. The CLGY463 line will be a valuable tool for this analysis, as it provides a visual marker for the relevant cell type.

Real-time analysis of CLGY463 showed a massive infiltration of YFP-positive neutrophils into injured tissue following dissection of the tip of the caudal fin. Transgenic zebrafish expressing GFP under control of the *mpx* (*mpo*) promoter were recently developed by others and also used to image neutrophilic inflammation of wounding sites [20,21]. To study possible functional differences between the YFP-positive neutrophil subpopulation in CLGY463 and other neutrophils during the inflammation process or its resolution, it would be useful that transgenic lines expressing cyan or red fluorescent proteins under control of the *mpx* promoter become available for crossing. Furthermore, construction of macrophage-specific marker lines would be very useful for comparative analyses.

Infection studies in CLGY463 using *E. coli*, *S. typhimurium* and *M. marinum* showed that both the YFP-positive neutrophils and many YFP-negative cells were attracted to infection sites. Within hours after infection, bacteria were mainly ingested by YFP-negative cells and partly by YFP-positive neutrophils. The YFP-negative population likely

consists of macrophages and possibly other neutrophils, since colocalization of *Salmonella* immunostaining with cells expressing either macrophage or neutrophil markers was observed. During the short-term response to infections it is impossible to distinguish if leukocyte migration is induced by microbial signals or by signals released from damaged tissue due to the injection. However, analysis of the long-term response to *M. marinum* infection clearly demonstrated the attraction of different leukocyte populations to infection foci. The association of YFP-positive neutrophils with *M. marinum*-induced granulomas in the zebrafish embryo is an interesting observation. Mycobacteria are known to target macrophages and escape intracellular killing [50]. The resulting host response in adult mammals is the aggregation of infected macrophages, neutrophils, dendritic cells, and T and B lymphocytes into granulomas [51]. Analysis in the zebrafish embryo model showed that innate immunity determinants are sufficient to initiate granuloma formation [15]. However, the contribution of neutrophils to granuloma formation and their role in control of mycobacterial infections has not been addressed in zebrafish and has raised some controversy in studies of mammalian models [52–57]. Different neutrophil depletion and transfusion studies in mice indicated a protective role for neutrophils in defense against mycobacterial infections [53–55]. This protective role was suggested to be of an immunomodulatory nature [54], since mycobacteria in several studies were not associated with neutrophils [54] or only during the first days after infection [52]. Others found that neutrophils had no protective effect against *M. tuberculosis* growth, but that neutrophil-mediated chemokine signaling was essential for accurate early granuloma formation [56]. Evidence for cooperation between macrophages and neutrophils in mycobacterial infections has also been reported [52,57]. Particularly, macrophages were shown to acquire granules from apoptotic neutrophils for antimicrobial activity against intracellular mycobacteria [57]. In the zebrafish model, we observed abundant mycobacteria that persisted for several days inside YFP-positive neutrophils, but also YFP-positive neutrophils without mycobacteria were associated with granulomas. Their presence might be suggestive of an immunomodulatory function. The transgenic zebrafish model described here provides a valuable tool to further address the role of neutrophils in mycobacterial infection, especially if used in combination with zebrafish mutants or bacterial mutants affected in granuloma formation.

Acknowledgments

We thank Helmut Brade (Research Center Borstel, Germany) for the Salmonella antibody, Hans de Bont (Leiden/Amsterdam Center for Drug Research, The Netherlands) for help with cell tracking, Ron Bout (Leiden Institute of Biology, The Netherlands) for help with Huygens software, Hilary Clay (University of Washington, USA) for advice on multiplex FISH, Kerstin Howe (Sanger Institute, UK) for advice on synteny, and Michael Redd (Huntsman Cancer Institute, USA) for helpful discussions on myeloid marker specificity. We are also grateful to Carina van der Laan, Fredericke Hannes, Merete Nilsen and Silke Rinkwitz for technical assistance and to Davy de Witt and Wim Schouten for fish maintenance. This work was supported by the European Commission 6th Framework Programme (LSHG-CT-2003-503496, ZF-MODELS) (A.H.M, H.P.S and T.S.B.), by The Netherlands Genomics Initiative (NROG, 050-71-001) (A.M.S. and W.B.), by the Sars Centre, University of Bergen (T.S.B), and by the National Programme in Functional Genomics in Norway (FUGE) in the Research Council of Norway (T.S.B.).

Appendix A. Supplementary materials

Supplementary data associated with this article can be found in the online version at doi:10.1016/j.dci.2007.04.003.

References

[1] Traver D, Herbomel P, Patton EE, Murphey RD, Yoder JA, Litman GW, et al. The zebrafish as a model organism to study development of the immune system. Adv Immunol 2003;81:253–330.
[2] Trede NS, Langenau DM, Traver D, Look AT, Zon LI. The use of zebrafish to understand immunity. Immunity 2004;20(4):367–79.
[3] Van der Sar AM, Appelmelk BJ, Vandenbroucke-Grauls CMJE, Bitter W. A star with stripes: zebrafish as an infection model. Trends Microbiol 2004;12(10):451–7.
[4] Berman JN, Kanki JP, Look AT. Zebrafish as a model for myelopoiesis during embryogenesis. Exp Hematol 2005;33(9):997–1006.
[5] Rhodes J, Hagen A, Hsu K, Deng M, Liu TX, Look AT, et al. Interplay of pu.1 and gata1 determines myelo-erythroid progenitor cell fate in zebrafish. Dev Cell 2005;8(1):97–108.
[6] Lieschke GJ, Oates AC, Paw BH, Thompson MA, Hall NE, Ward AC, et al. Zebrafish SPI-1 (PU.1) marks a site of myeloid development independent of primitive erythropoiesis: implications for axial patterning. Dev Biol 2002;246(2):274–95.
[7] Herbomel P, Thisse B, Thisse C. Ontogeny and behaviour of early macrophages in the zebrafish embryo. Development 1999;126(17):3735–45.
[8] Willett CE, Cortes A, Zuasti A, Zapata AG. Early hematopoiesis and developing lymphoid organs in the zebrafish. Dev Dynamics 1999;214(4):323–36.
[9] Bennett CM, Kanki JP, Rhodes J, Liu TX, Paw BH, Kieran MW, et al. Myelopoiesis in the zebrafish, *Danio rerio*. Blood 2001;98(3):643–51.
[10] Herbomel P, Thisse B, Thisse C. Zebrafish early macrophages colonize cephalic mesenchyme and developing brain, retina, and epidermis through a M-CSF receptor-dependent invasive process. Dev Biol 2001;238(2):274–88.
[11] Lieschke GJ, Oates AC, Crowhurst MO, Ward AC, Layton JE. Morphologic and functional characterization of granulocytes and macrophages in embryonic and adult zebrafish. Blood 2001;98(10):3087–96.
[12] Crowhurst MO, Layton JE, Lieschke GJ. Developmental biology of zebrafish myeloid cells. Int J Dev Biol 2002;46(4):483–92.
[13] Davidson AJ, Zon LI. The 'definitive' (and 'primitive') guide to zebrafish hematopoiesis. Oncogene 2004;23(43):7233–46.
[14] Lam SH, Chua HL, Gong Z, Lam TJ, Sin YM. Development and maturation of the immune system in zebrafish, *Danio rerio*: a gene expression profiling, in situ hybridization and immunological study. Dev Comp Immunol 2004;28(1):9–28.
[15] Davis JM, Clay H, Lewis JL, Ghori N, Herbomel P, Ramakrishnan L. Real-time visualization of mycobacterium-macrophage

interactions leading to initiation of granuloma formation in zebrafish embryos. Immunity 2002;17(6):693–702.
[16] Ward AC, McPhee DO, Condron MM, Varma S, Cody SH, Onnebo SM, et al. The zebrafish spi1 promoter drives myeloid-specific expression in stable transgenic fish. Blood 2003;102(9): 3238–40.
[17] Hsu K, Traver D, Kutok JL, Hagen A, Liu TX, Paw BH, et al. The pu.1 promoter drives myeloid gene expression in zebrafish. Blood 2004;104(5):1291–7.
[18] Lawson ND, Weinstein BM. In vivo imaging of embryonic vascular development using transgenic zebrafish. Dev Biol 2002;248(2):307–18.
[19] Redd MJ, Kelly G, Dunn G, Way M, Martin P. Imaging macrophage chemotaxis in vivo: studies of microtubule function in zebrafish wound inflammation. Cell Motil Cytoskeleton 2006;63(7):415–22.
[20] Mathias JR, Perrin BJ, Liu TX, Kanki J, Look AT, Huttenlocher A. Resolution of inflammation by retrograde chemotaxis of neutrophils in transgenic zebrafish. J Leukoc Biol 2006;80(6): 1281–8.
[21] Renshaw SA, Loynes CA, Trushell DM, Elworthy S, Ingham PW, Whyte MK. A transgenic zebrafish model of neutrophilic inflammation. Blood 2006;108(13):3976–8.
[22] Bellen HJ. Ten years of enhancer detection: lessons from the fly. Plant Cell 1999;11(12):2271–81.
[23] Amsterdam A, Becker TS. Transgenes as screening tools to probe and manipulate the zebrafish genome. Dev Dynamics 2005;234(2):255–68.
[24] Ellingsen S, Laplante MA, Konig M, Kikuta H, Furmanek T, Hoivik EA, et al. Large-scale enhancer detection in the zebrafish genome. Development 2005;132(17):3799–811.
[25] Laplante M, Kikuta H, Konig M, Becker TS. Enhancer detection in the zebrafish using pseudotyped murine retroviruses. Methods 2006;39(3):189–98.
[26] Meijer AH, Krens SFG, Medina Rodriguez IA, He S, Bitter W, Snaar-Jagalska BE, et al. Expression analysis of the Toll-like receptor and TIR domain adaptor families of zebrafish. Mol Immunol 2004;40(11):773–83.
[27] Thisse C, Thisse B, Schilling TF, Postlethwait JH. Structure of the zebrafish snail1 gene and its expression in wild-type, spadetail and no tail mutant embryos. Development 1993; 119(4):1203–15.
[28] Clay H, Ramakrishnan L. Multiplex fluorescent in situ hybridization in zebrafish embryos using tyramide signal amplification. Zebrafish 2005;2(2):105–11.
[29] Welten MCM, de Haan SB, Van den Boogert N, Noordermeer JN, Lamers GEM, Spaink HP, et al. ZebraFISH: fluorescent in situ hybridization protocol and three-dimensional imaging of gene expression patterns. Zebrafish 2006;3(4):465–76.
[30] Stuurman N, Pacios BC, Schlaman HR, Wijfjes AH, Bloemberg G, Spaink HP. Use of green fluorescent protein color variants expressed on stable broad-host-range vectors to visualize rhizobia interacting with plants. Mol Plant Microbe Interact 2000;13(11):1163–9.
[31] Shaner NC, Campbell RE, Steinbach PA, Giepmans BN, Palmer AE, Tsien RY. Improved monomeric red, orange and yellow fluorescent proteins derived from *Discosoma* sp. red fluorescent protein. Nat Biotechnol 2004;22(12):1567–72.
[32] Van der Sar AM, Abdallah AM, Sparrius M, Reinders E, Vandenbroucke-Grauls CM, Bitter W. *Mycobacterium marinum* strains can be divided into two distinct types based on genetic diversity and virulence. Infect Immun 2004;72(11): 6306–12.
[33] Hayward CM, O'Gaora P, Young DB, Griffin GE, Thole J, Hirst TR, et al. Construction and murine immunogenicity of recombinant Bacille-Calmette–Guerin vaccines expressing the B subunit of *E. coli* heat labile enterotoxin. Vaccine 1999; 17(9–10):1272–81.
[34] Murayama E, Kissa K, Zapata A, Mordelet E, Briolat V, Lin HF, et al. Tracing hematopoietic precursor migration to successive hematopoietic organs during zebrafish development. Immunity 2006;25(6):963–75.
[35] Lin HF, Traver D, Zhu H, Dooley K, Paw BH, Zon LI, et al. Analysis of thrombocyte development in CD41-GFP transgenic zebrafish. Blood 2005;106(12):3803–10.
[36]. Thisse B, Thisse C. Fast Release Clones: A high throughput expression analysis. ZFIN Direct Data Submission 2004; 〈http://ZFIN.org〉: ZDB-PUB-040907-1.
[37] Loeb-Hennard C, Kremmer E, Bally-Cuif L. Prominent transcription of zebrafish N-myc (nmyc1) in tectal and retinal growth zones during embryonic and early larval development. Gene Expression Patterns 2005;5(3):341–7.
[38] Liu F, Wen Z. Cloning and expression pattern of the lysozyme C gene in zebrafish. Mech Dev 2002;113(1): 69–72.
[39] Parichy DM, Ransom DG, Paw B, Zon LI, Johnson SL. An orthologue of the kit-related gene fms is required for development of neural crest-derived xanthophores and a subpopulation of adult melanocytes in the zebrafish, *Danio rerio*. Development 2000;127(14):3031–44.
[40] Van der Sar AM, Musters RJ, van Eeden FJ, Appelmelk BJ, Vandenbroucke-Grauls CM, Bitter W. Zebrafish embryos as a model host for the real time analysis of *Salmonella typhimurium* infections. Cell Microbiol 2003;5(9):601–11.
[41] Godin I, Cumano A. The hare and the tortoise: an embryonic haematopoietic race. Nat Rev Immunol 2002;2(8): 593–604.
[42] Detrich III HW, Kieran MW, Chan FY, Barone LM, Yee K, Rundstadler JA, et al. Intraembryonic hematopoietic cell migration during vertebrate development. Proc Natl Acad Sci USA 1995;92(23):10713–7.
[43] Klebanoff SJ. Myeloperoxidase: friend and foe. J Leukoc Biol 2005;77(5):598–625.
[44] Schreiber-Agus N, Horner J, Torres R, Chiu FC, DePinho RA. Zebra fish myc family and max genes: differential expression and oncogenic activity throughout vertebrate evolution. Mol Cell Biol 1993;13(5):2765–75.
[45] Hoffman B, Amanullah A, Shafarenko M, Liebermann DA. The proto-oncogene c-myc in hematopoietic development and leukemogenesis. Oncogene 2002;21(21):3414–21.
[46] Hooker CW, Hurlin PJ. Of Myc and Mnt. J Cell Sci 2006;119 (Part 2):208–16.
[47] Johansen LM, Iwama A, Lodie TA, Sasaki K, Felsher DW, Golub TR, et al. c-Myc is a critical target for c/EBPalpha in granulopoiesis. Mol Cell Biol 2001;21(11):3789–806.
[48] Lyons SE, Shue BC, Lei L, Oates AC, Zon LI, Liu PP. Molecular cloning, genetic mapping, and expression analysis of four zebrafish c/ebp genes. Gene 2001;281(1–2): 43–51.
[49] Lyons SE, Shue BC, Oates AC, Zon LI, Liu PP. A novel myeloid-restricted zebrafish CCAAT/enhancer-binding protein with a potent transcriptional activation domain. Blood 2001;97(9): 2611–7.
[50] van Crevel R, Ottenhoff TH, Van der Meer JW. Innate immunity to *Mycobacterium tuberculosis*. Clin Microbiol Rev 2002;15(2): 294–309.
[51] Tsai MC, Chakravarty S, Zhu G, Xu J, Tanaka K, Koch C, et al. Characterization of the tuberculous granuloma in murine and human lungs: cellular composition and relative tissue oxygen tension. Cell Microbiol 2006;8(2):218–32.
[52] Silva MT, Silva MN, Appelberg R. Neutrophil-macrophage cooperation in the host defence against mycobacterial infections. Microb Pathogenesis 1989;6(5):369–80.
[53] Appelberg R, Castro AG, Gomes S, Pedrosa J, Silva MT. Susceptibility of beige mice to *Mycobacterium avium*: role of neutrophils. Infect Immun 1995;63(9):3381–7.

[54] Pedrosa J, Saunders BM, Appelberg R, Orme IM, Silva MT, Cooper AM. Neutrophils play a protective nonphagocytic role in systemic *Mycobacterium tuberculosis* infection of mice. Infect Immun 2000;68(2):577–83.

[55] Fulton SA, Reba SM, Martin TD, Boom WH. Neutrophil-mediated mycobacteriocidal immunity in the lung during *Mycobacterium bovis* BCG infection in C57BL/6 mice. Infect Immun 2002; 70(9):5322–7.

[56] Seiler P, Aichele P, Bandermann S, Hauser AE, Lu B, Gerard NP, et al. Early granuloma formation after aerosol *Mycobacterium tuberculosis* infection is regulated by neutrophils via CXCR3-signaling chemokines. Eur J Immunol 2003;33(10):2676–86.

[57] Tan BH, Meinken C, Bastian M, Bruns H, Legaspi A, Ochoa MT, et al. Macrophages acquire neutrophil granules for antimicrobial activity against intracellular pathogens. J Immunol 2006; 177(3):1864–71.